

Structure of the He^3 Nucleus*†

H. COLLARD AND R. HOFSTADTER

Department of Physics and High-Energy Physics Laboratory, Stanford University, Stanford, California

(Received 18 February 1963)

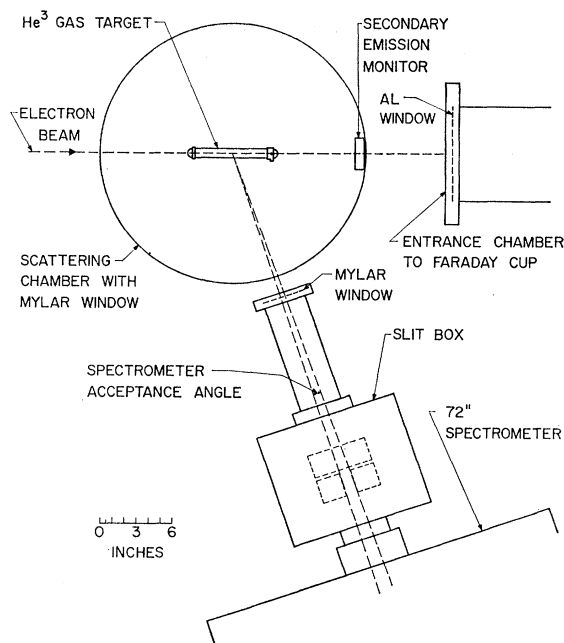
The He^3 nucleus has been investigated by means of the elastic electron scattering technique. Experiments were carried out in the energy range 110–650 MeV. Absolute differential cross sections were measured at angles lying between 40° and 135° in the above energy range. Form factors were observed for both the charge density and magnetic moment density of the He^3 nucleus. The results indicate that the charge cloud may be represented best by a model similar to a hollow exponential I type of rms radius 2.05 F. The magnetic moment cloud can be represented approximately by a Gaussian model of rms radius 1.66 F. There appears to be a difference between the gross features of the charge and magnetic moment clouds, and the magnetic moment cloud appears to be the more compact of the two.

I. INTRODUCTION

THE two important elements permitting an investigation of the nuclear three-body problem are the mirror-nuclei ${}^1_1\text{H}^3$ and ${}^2_2\text{He}^3$. The electron-scattering technique is highly suitable for the study of the simple combinations of nucleons in these elements. Information about the ground-state wave functions can be derived from the elastic scattering results. Inelastic scattering cross sections will yield complementary data on the momentum distribution of the nucleons in the ground state as well as on transitions to excited states of varying stability. Time-coincidence investigations between ejected protons or neutrons and the residual fragments of the initial nuclei can furnish important clues to relative correlations of the particles in these nuclei. Proton and neutron form factors can be investigated in the bound state in the relatively simple nuclei of H^3 and He^3 . In addition, electroproduction of neutral and charged pions can be examined under the relatively simple conditions prevailing in these light three-body nuclei. Finally, the series of nuclides ${}^1_1\text{H}^1$, ${}^1_1\text{H}^2$, ${}^1_1\text{H}^3$, ${}^2_2\text{He}^3$, ${}^2_2\text{He}^4$ offers an unrivalled opportunity to study the relative changes occurring when the number of nucleons changes by one and two units, thus allowing tests of the charge-independent nature of nucleon forces to be scrutinized under carefully controlled conditions. All the above information, when available, will certainly help to throw light on the question of whether there is or is not an intrinsic nuclear three-body force. The richness of this field of study is evident to us and we have selected the nuclide He^3 to begin such a series of investigations. At the present time, in collaboration with the Los Alamos Scientific Laboratory, we are also preparing a parallel series of experiments on H^3 . In this paper, we discuss our recent work on the nucleus He^3 .

II. APPARATUS

The present experiments have been carried out on gaseous He^3 . We have employed a technique similar to one used previously^{1,2} in numerous experiments on He^4 . The target consists of a thin cylinder made of stainless steel carrying thin end caps through which the main beam enters and leaves the cell. Because of the relative scarcity of He^3 gas we used a target with walls sufficiently thick to guarantee the safety of the gas in the target. Hence, we used 20 mil as wall thickness of the cylindrical part of the target and 10-mil end caps made in the form of hemispheres. A diagram of the target and scattering chamber is shown in Fig. 1. Pressures of He^3 gas up to 1125 psi were used.

FIG. 1. The He^3 target and scattering chamber.

* This work was supported in part by the U. S. Office of Naval Research, the U. S. Atomic Energy Commission, and the U. S. Air Force Office of Scientific Research.

† A preliminary account of this work was presented at the Seattle Meeting of the American Physical Society [Bull. Am. Phys. Soc. 7, 489 (1962)].

¹ R. McAllister and R. Hofstadter, Phys. Rev. **102**, 851 (1956).

² G. R. Bureson, Phys. Rev. **121**, 624 (1961).

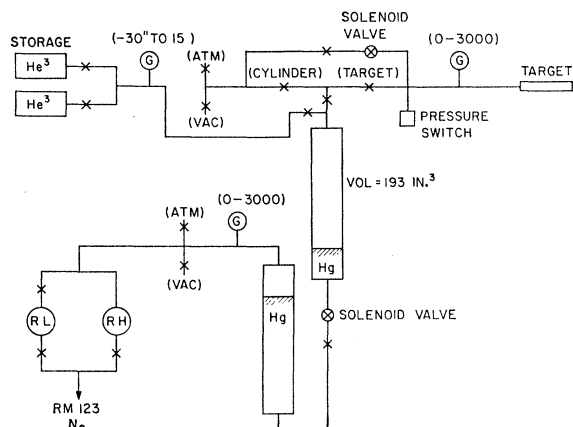


FIG. 2. A schematic diagram of the filling system of the target vessel.

To make it easier to obtain absolute cross sections a companion target of ordinary hydrogen gas was used in an identical target cell. In this case pressures up to 1800 psi were used. Alternate measurements were made in which the He^3 data were observed under the same conditions as those of the comparison H_2 target. Gas pressures in both targets were monitored continuously. Known proton cross sections³ were used as calibration data to calculate He^3 cross sections. The He^3 gas target was filled by means of a Toepler pump. The schematic diagram of this apparatus is shown in Fig. 2. Filling of the He^3 target to pressures of 1000 psi from two 6.5 liter cylinders at 1.0 atm took but six "pushes" and involved about 2 h of filling time.

Both the 36- and 72-in. spectrometers⁴ were used independently to take data on cross sections. Samples of the results are shown in Fig. 3.

In many cases it has been necessary to extrapolate the inelastic continuum underneath the elastic peak in order to obtain the area under the He^3 peak. An example is shown in Fig. 3. We have been aided in this procedure by the appearance of the right-hand side of the peak, which should be affected very little by the inelastic continuum. The errors placed on experimental points have been chosen to be large enough to take care of the uncertainty in this extrapolation procedure. It is seen below that the errors are reasonably small except in the case of the analysis of the magnetic scattering from He^3 .

Because the radiative effects are so similar for He^3 and H^1 we have not made any relative corrections in obtaining absolute cross sections. We estimate that no errors larger than two percent are introduced by neglecting such corrections.

³ F. Bumiller, M. Croissiaux, E. Dally, and R. Hofstadter, *Phys. Rev.* **124**, 1623 (1961).

⁴ R. Hofstadter, F. A. Bumiller, B. R. Chambers, and M. Croissiaux, in *Proceedings of an International Conference on Instrumentation for High-Energy Physics* (Interscience Publishers, Inc., New York, 1960), p. 310.

III. ANALYSIS OF THE EXPERIMENTAL RESULTS

He^3 is a nucleus light enough so that the scattering from its magnetic moment can be observed easily. It has been possible for us also to study the dynamic behavior of its magnetic moment. By this we mean that the form factor of the magnetic moment of He^3 can be measured under nonstatic conditions (momentum transfer $>$ zero).

A first Born approximation phenomenological theory of the elastic scattering of high-energy electrons from He^3 can be stated in terms of a Rosenbluth-like expression for the cross section:

$$\frac{d\sigma}{d\Omega} / \left(\frac{Ze^2}{2E} \right)^2 \frac{\cos^2(\theta/2)}{\sin^4(\theta/2)} \frac{1}{1 + (2E/Mc^2) \sin^2(\theta/2)} = G$$

$$= F_1^2 + \frac{\hbar^2 q^2}{4M^2 c^2} [2(F_1 + KF_2)^2 \tan^2(\theta/2) + K^2 F_2^2], \quad (1)$$

when F_1 and F_2 are "Dirac" and "Pauli" form factors which are functions of the momentum transfer, $\hbar q$, given by

$$q = \frac{(2E/\hbar c) \sin(\theta/2)}{[1 + (2E/Mc^2) \sin^2(\theta/2)]^{1/2}}. \quad (2)$$

In this equation the parameters for He^3 have the values

$$Z = 2,$$

$$Mc^2 = 2808 \text{ MeV}, \quad (3)$$

$$K = -4.20 \text{ He}^3 \text{ magnetons}.$$

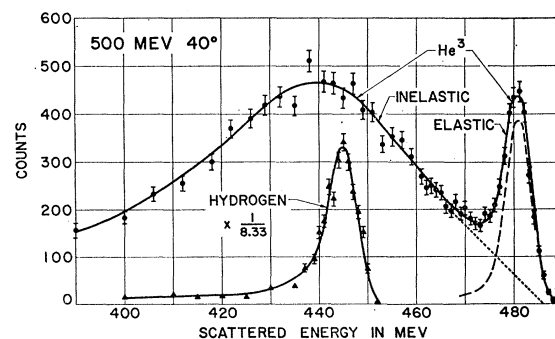
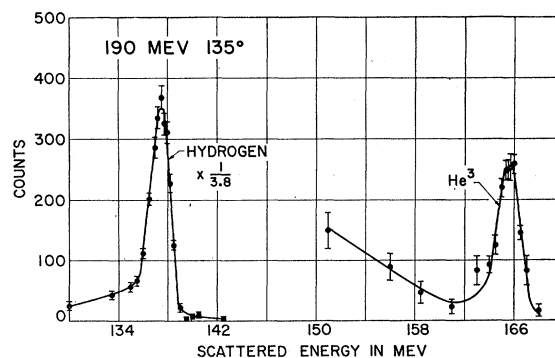
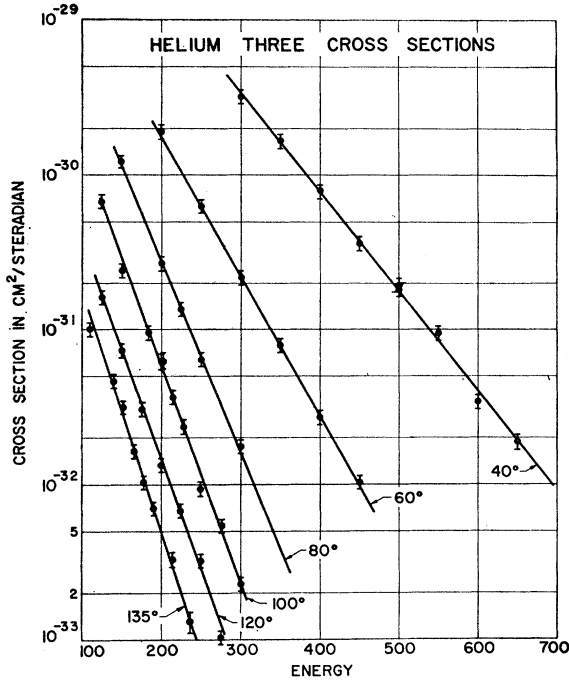


FIG. 3. Two examples of He^3 data and of comparison H data.

FIG. 4. He³ elastic cross sections.

For the proton the corresponding parameters are

$$\begin{aligned} Z &= 1, \\ Mc^2 &= 938 \text{ MeV}, \\ K &= 1.79 \text{ nuclear magnetons.} \end{aligned} \quad (4)$$

The use of the Rosenbluth equation is justified since Yennie *et al.*⁵ have shown that this equation applies to any particle having a spin of $\frac{1}{2}\hbar$. The spin of He³ is indeed $\frac{1}{2}\hbar$. It is possible to express the results for He³ in terms of the form factors F_{ch} and F_{mag} given below⁵⁻⁸:

$$F_{\text{ch}} = F_1 - (\hbar^2 q^2 / 4M^2 c^2) K F_2, \quad (5)$$

$$F_{\text{mag}} = (F_1 + K F_2) / (1 + K). \quad (6)$$

These form factors are very similar to F_1 and F_2 because $M^2 c^2$ is very large for He³ and K is also quite large compared with unity. Our results are given below both in terms of F_1 and F_2 and in terms of F_{ch} and F_{mag} .

It remains, of course, for experiment to determine whether Eq. (1) can be applied consistently and successfully to the data. It is desirable for this purpose to make consistency checks to determine whether F_1 and F_2 are functions *only* of q as they are required to be in the formulation of the phenomenological theory underlying Eq. (1). Such tests can be made by plotting

⁵ D. R. Yennie, M. M. Lévy, and D. G. Ravenhall, *Rev. Mod. Phys.* **29**, 144 (1957).

⁶ R. G. Sachs, *Phys. Rev.* **126**, 2256 (1962).

⁷ J. D. Walecka (private communication).

⁸ L. N. Hand, D. G. Miller, and R. Wilson, *Phys. Rev. Letters* **8**, 110 (1962).

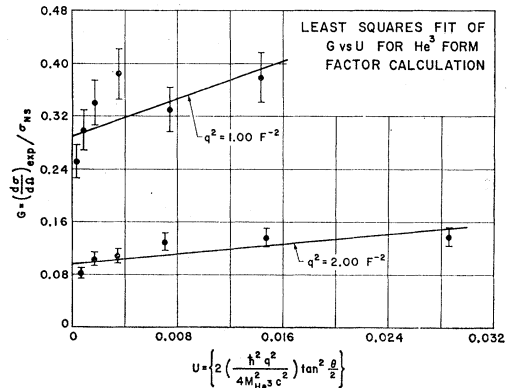
G , i.e., the elastic cross section divided by the Mott point cross in Eq. (1), against $\tan^2(\theta/2)$. A straight line passing through the experimental data points would prove the internal consistency of the theory. As is well known, a straight line in this type of plot is equivalent to a single point of intersection (or a small region, within experimental error) in the "method of intersecting ellipses."^{9,10} We comment below on the results of such tests.

In actuality the exact phase-shift method¹¹ should be applied to the scattering process which would be an improvement over the first Born approximation. Estimates of the small errors involved in using the first Born approximation can be made by using the Feshbach-McKinley theory¹² which indicates errors of 2% at 135° and 1% at 40°. These errors are small compared with the present experimental error and are neglected. However, they should be kept in mind for subsequent measurements which no doubt will be made with higher precision.

IV. RESULTS

The cross sections for elastic scattering of high-energy electrons from He³ gas were measured at incident energies lying between 110 MeV and 650 MeV. Laboratory scattering angles varied between 40° and 135°. The complete set of measured points is shown in Fig. 4. Table I gives the values of the numerical results. The appropriate values of q^2 vary between 1.0 and 5.0 F⁻².

In Fig. 4 the solid lines represent empirical fits to the data made by a visual analysis. On semilog paper

FIG. 5. Straight-line plots of $\tan^2(\theta/2)$ data at $q^2 = 1.0$ and 2.0 F^{-2} .

⁹ R. Hofstadter, in *Proceedings of the Ninth International Annual Conference on High-Energy Physics* (Academy of Sciences, Moscow, USSR, 1960), Vol. I, p. 355.

¹⁰ R. Herman and R. Hofstadter, *High Energy Electron Scattering Tables* (Stanford University Press, Stanford, California, 1960), p. 37.

¹¹ L. R. B. Elton, *Proc. Phys. Soc. (London)* **A63**, 1115 (1950); D. R. Yennie, D. G. Ravenhall, and R. N. Wilson, *Phys. Rev.* **95**, 500 (1954).

¹² W. A. McKinley, Jr., and H. Feshbach, *Phys. Rev.* **74**, 1759 (1948).

TABLE I. He³ cross sections for elastic scattering of electrons.

E_0 (MeV)	θ_{lab}	q^2 (F ⁻²)	$d\sigma/d\Omega$ (cm ² /sr)
300	40	1.06	$(3.21 \pm 0.32) \times 10^{-30}$
350	40	1.43	$(1.65 \pm 0.17) \times 10^{-30}$
400	40	1.86	$(7.80 \pm 0.78) \times 10^{-31}$
450	40	2.35	$(3.59 \pm 0.36) \times 10^{-31}$
500	40	2.89	$(1.92 \pm 0.19) \times 10^{-31}$
500	40	2.89	$(1.81 \pm 0.18) \times 10^{-31}$
550	40	3.48	$(9.40 \pm 0.94) \times 10^{-32}$
600	40	4.13	$(3.38 \pm 0.34) \times 10^{-32}$
650	40	4.83	$(1.85 \pm 0.19) \times 10^{-32}$
200	60	0.99	$(1.90 \pm 0.19) \times 10^{-30}$
250	60	1.54	$(6.27 \pm 0.63) \times 10^{-31}$
300	60	2.20	$(2.16 \pm 0.22) \times 10^{-31}$
350	60	2.96	$(7.95 \pm 0.80) \times 10^{-32}$
400	60	3.84	$(2.69 \pm 0.27) \times 10^{-32}$
450	60	4.82	$(1.03 \pm 0.10) \times 10^{-32}$
150	80	0.92	$(1.22 \pm 0.12) \times 10^{-30}$
200	80	1.60	$(2.67 \pm 0.27) \times 10^{-31}$
225	80	2.02	$(1.35 \pm 0.14) \times 10^{-31}$
250	80	2.48	$(6.37 \pm 0.64) \times 10^{-32}$
300	80	3.52	$(1.76 \pm 0.18) \times 10^{-32}$
125	100	0.90	$(6.79 \pm 0.68) \times 10^{-31}$
150	100	1.28	$(2.43 \pm 0.24) \times 10^{-31}$
183	100	1.88	$(9.45 \pm 0.95) \times 10^{-32}$
198	100	2.18	$(6.13 \pm 0.61) \times 10^{-32}$
200	100	2.23	$(6.15 \pm 0.62) \times 10^{-32}$
214	100	2.54	$(3.65 \pm 0.37) \times 10^{-32}$
228	100	2.86	$(2.36 \pm 0.24) \times 10^{-32}$
250	100	3.42	$(9.32 \pm 0.93) \times 10^{-33}$
275	100	4.10	$(5.42 \pm 0.54) \times 10^{-33}$
300	100	4.84	$(2.28 \pm 0.23) \times 10^{-33}$
125	120	1.12	$(1.62 \pm 0.16) \times 10^{-31}$
150	120	1.60	$(7.32 \pm 0.73) \times 10^{-32}$
175	120	2.16	$(3.08 \pm 0.31) \times 10^{-32}$
200	120	2.78	$(1.34 \pm 0.14) \times 10^{-32}$
225	120	3.50	$(6.87 \pm 0.69) \times 10^{-33}$
250	120	4.26	$(3.25 \pm 0.33) \times 10^{-33}$
275	120	5.09	$(1.03 \pm 0.11) \times 10^{-33}$
110	135	1.00	$(1.01 \pm 0.10) \times 10^{-31}$
140	135	1.58	$(4.67 \pm 0.47) \times 10^{-32}$
153	135	1.88	$(3.17 \pm 0.32) \times 10^{-32}$
166	135	2.20	$(1.65 \pm 0.17) \times 10^{-32}$
178	135	2.51	$(1.05 \pm 0.11) \times 10^{-32}$
190	135	2.84	$(7.13 \pm 0.70) \times 10^{-33}$
214	135	3.56	$(3.32 \pm 0.33) \times 10^{-33}$
237	135	4.31	$(1.31 \pm 0.20) \times 10^{-33}$
250	135	4.77	$(7.64 \pm 1.15) \times 10^{-34}$

the fits to the cross sections are given essentially by straight lines.

In Figs. 5-8 we give the results for G of Eq. (1) obtained from Fig. 4 or Table I. The solid lines refer to least-square fits to the experimental points. It may be noted that, by and large, straight lines can be used to fit the data. However, there does seem to be a small

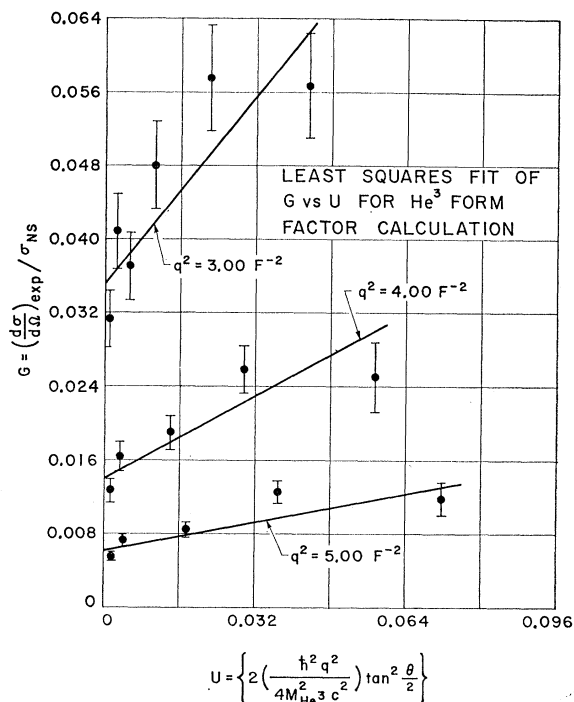


Fig. 6. Straight-line plots of $\tan^2(\theta/2)$ data at $q^2 = 3.0, 4.0,$ and 5.0 F⁻².

but systematic deviation of the measured values away from straight lines. The experimental points tend to show a slight bulge above the mean square fits in all cases. Whether such deviations are real or not cannot be determined definitely at the present time. It would be interesting to know in which direction the phase-shift results would modify the behavior of the $\tan^2(\theta/2)$ plots.

The data in Figs. 5-8 yield values of F_1 and F_2 (and also F_{ch} and F_{mag}). The results are given in Figs. 9 and 10 and in Table II. The errors in F_2 are rather

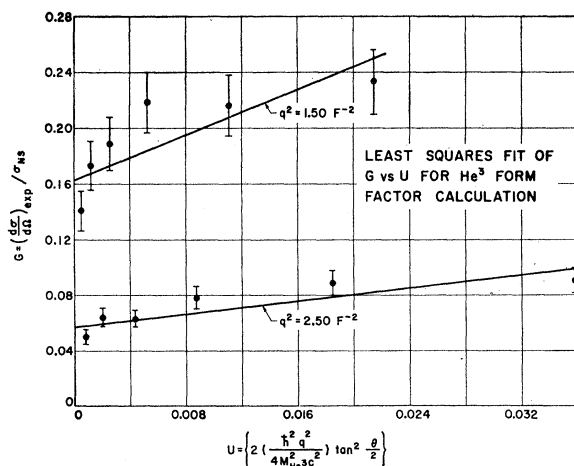


Fig. 7. Straight line plots of $\tan^2(\theta/2)$ data at $q^2 = 1.5$ and 2.5 F⁻².

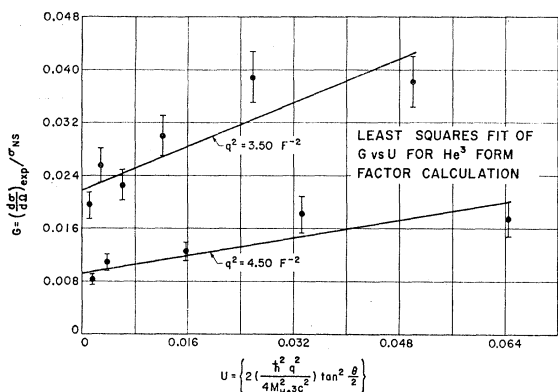


FIG. 8. Straight line plots of $\tan^2(\theta/2)$ data at $q^2 = 3.5$ and $4.5 F^{-2}$.

large at small values of q^2 , for in this region the magnetic scattering is relatively small compared with charge scattering. To see how well these calculated form factors fit the original experimental observations, we show in Fig. 11 the cross sections calculated from Eqs. (1), (2), and (3) by employing the experimental form factors of Figs. 9 and 10 and Table II. The triangles show the recomputed values and the circles (with margins of error) the actual cross sections. As observed previously the fit is quite good but not perfect. Perhaps the deviations from the straight lines in the $\tan^2(\theta/2)$ plots are responsible for the imperfection of the fit. The principal results of the experiment are summarized in Figs. 9 and 10 and in Table II.

TABLE II. He^3 form factors.

q^2 (F^{-2})	F_1	F_2	F_{ch}	F_{mag}
1.0	0.527 ± 0.013	0.759 ± 0.118	0.531 ± 0.013	0.832 ± 0.146
1.5	0.390 ± 0.009	0.571 ± 0.060	0.395 ± 0.009	0.628 ± 0.076
2.0	0.298 ± 0.008	0.401 ± 0.042	0.302 ± 0.008	0.433 ± 0.053
2.5	0.227 ± 0.006	0.314 ± 0.026	0.231 ± 0.006	0.341 ± 0.032
3.0	0.178 ± 0.005	0.233 ± 0.020	0.182 ± 0.005	0.244 ± 0.021
3.5	0.138 ± 0.004	0.186 ± 0.014	0.142 ± 0.004	0.194 ± 0.018
4.0	0.109 ± 0.004	0.152 ± 0.013	0.112 ± 0.004	0.165 ± 0.016
4.5	0.088 ± 0.003	0.119 ± 0.011	0.091 ± 0.003	0.129 ± 0.013
5.0	0.072 ± 0.002	0.091 ± 0.008	0.075 ± 0.002	0.097 ± 0.010

It may be noticed that F_2 is larger than F_1 . This is at first sight an unexpected result because one usually thinks of noncancelling currents as spread out over the surfaces of nuclei. The fact that F_2 (or F_{mag}) is larger than F_1 (or F_{ch}), on the other hand, suggests that the distribution of magnetism is less spread out than the charge. This result is borne out by the interpretive studies made in the next section.

Before going to those studies, the result that $F_2 > F_1$ may indicate that the magnetic moment associated with the neutron appears in an orbit somewhat more

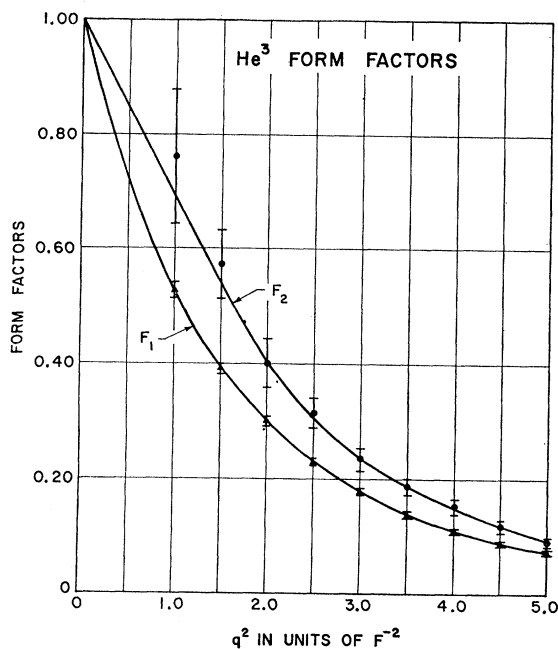


FIG. 9. Plots of F_1 and F_2 for He^3 .

restricted than that of the protons. In making this hypothesis we assume that the magnetic moment of He^3 in the ground state is mainly associated with the neutron. We wonder also whether the fact that there are *two* protons to account for the charge and only *one* neutron to account for the magnetic moment may not be connected with the observation that $F_2 > F_1$. Perhaps the spin-spin forces can account for such a result. In

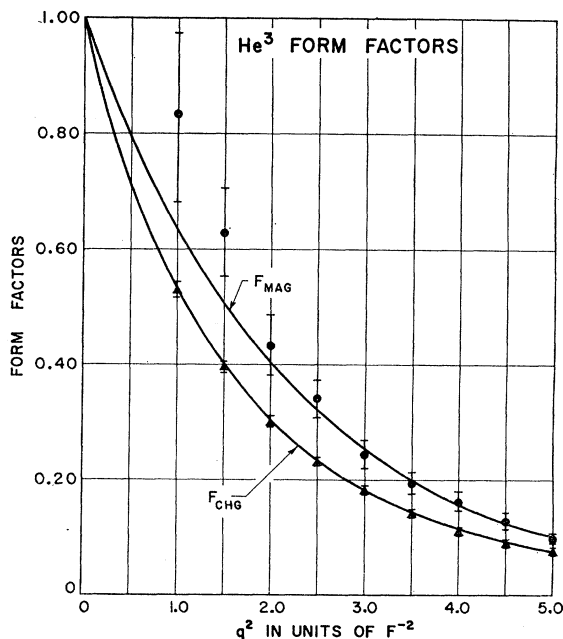


FIG. 10. Plots of F_{ch} and F_{mag} for He^3 .

any case we should like to call attention to the difference between F_2 and F_1 and hope that theory may soon yield an explanation of this interesting phenomenon.

V. INTERPRETATION OF FORM FACTORS

We have attempted to fit our observed form factors by using the usual first Born approximation formula which gives the form factor as a Fourier transform of the charge or magnetic moment distribution. Many models have been tried but we report here only on the more successful fits that have been obtained.

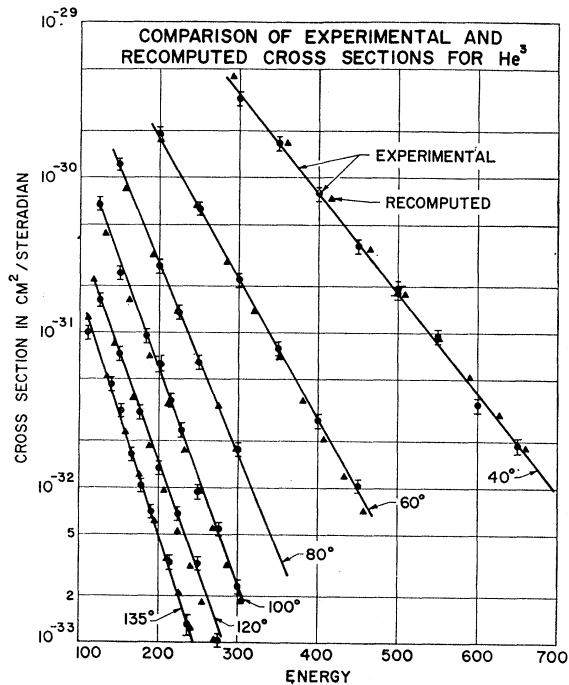


FIG. 11. Comparison of experimental and recomputed cross sections.

Figure 12 shows a comparison between experimental data for F_1 and one of the simplest of successful models, the Gaussian model. The solid lines in Fig. 12 correspond to Gaussian models with the rms radii indicated. Though the fit is not perfect the general tendency appears to be correct. Figure 13 gives the corresponding results for F_2 for Gaussian models of the appropriate rms radii. Again the fit is not perfect, but the general behavior of the model is correct. Note that the radii for the "successful" Gaussian models for charge and magnetic moment distributions differ and that the rms magnetic radius $a_2 \approx 1.68 F$ is smaller than the rms charge radius $a_1 \approx 1.86 F$. The corresponding results for F_{mag} and F_{ch} differ very little from the above results and yield $a_{\text{mag}} \approx 1.66 F$ and $a_{\text{ch}} \approx 1.85 F$.

In Figs. 14 and 15 we show similar results for a hollow exponential I model⁹ for the He³ nucleus. In this case the fits for F_1 and F_{ch} show some improvement

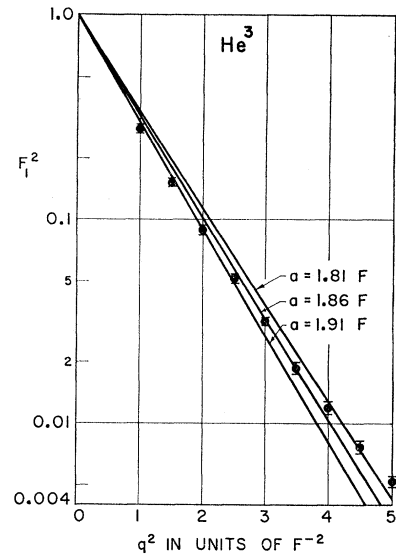


FIG. 12. Gaussian fits to F_1 .

with respect to a Gaussian model and the appropriate rms radii are close to $a_1 = 2.07 F$, and $a_{\text{ch}} = 2.05 F$. For F_2 and F_{mag} the hollow exponential I does not fit as well as in the case of F_1 or F_{ch} but the rms radii are, respectively, ~ 1.85 and $\sim 1.82 F$. Thus, we see a reflection of the same fact in this second model that the charge cloud is larger in extent than the magnetic moment cloud. In fact, relatively good fits are given by the hollow exponential I for the charge and by the Gaussian for the magnetic moment.

Other phenomenological models have been tried and the results are shown in Table III. Among all the models we have examined the hollow exponential appears to fit the best in the case of the charge distribution. Of course, we do not take this model literally, and any model that is not too highly peaked in the middle ($r=0$) will suffice if the rest of the model is approximately like that of the hollow exponential. We

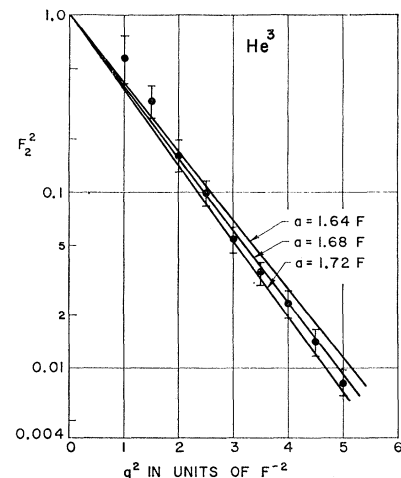


FIG. 13. Gaussian fits to F_2 .

TABLE III. Rms radii (in F) for various successful^a form factor models.

Model	a_1	a_2	a_{ch}	a_{mag}
Gaussian	1.86 (mediocre fit)	1.68	1.85 (mediocre fit)	1.66
Harmonic well	...	1.65 ($\alpha = \frac{1}{3}$)	...	1.63 ($\alpha = \frac{1}{3}$)
Hollow exponential I	2.07	1.85 (poor fit)	2.05	1.82 (poor fit)
Hollow exponential II	...	1.75	...	1.73
Modified harmonic well	2.04 ($\alpha_1=0.93, \alpha_2=0.40$)	1.66 ($\alpha_1=0.87, \alpha_2=0.54$)	2.03 ($\alpha_1=0.93, \alpha_2=0.40$)	1.64 ($\alpha_1=0.87, \alpha_2=0.54$) ^a

^a Unsuccessful models tried were the uniform, exponential, shell, Yukawa I*, Yukawa II*, hollow Gaussian, modified exponential I, and Clementel-Villi. (See reference 10, pp. 16-23 and 116-181.)

have commented on this type of result before when we studied the lithium nucleus.¹³ We illustrate the above remarks by plotting (in Fig. 16) $4\pi r^2 \rho$ against r for the two models discussed above.

VI. CONCLUDING REMARKS

Our results in He³ show a general agreement with the phenomenological Rosenbluth equation but not perfect agreement. The magnetic radius of He³ is smaller than the charge radius. A reasonable value for the charge radius is $a_{ch}=2.05$ F (hollow exponential I model) and a reasonable value for the magnetic radius is $a_{mag}=1.66$ F (Gaussian model). The errors in the above determinations are difficult to estimate but we believe that a $\pm 10\%$ error on each radius is generous. The above values are not corrected for the finite size of the proton. When such a correction is made the

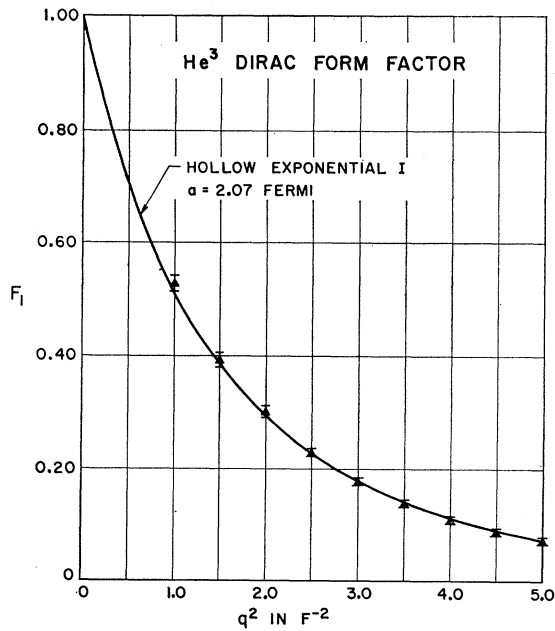


FIG. 14. Hollow exponential I fit to F_1 .

¹³ G. R. Bureson and R. Hofstadter, Phys. Rev. **112**, 1282 (1958).

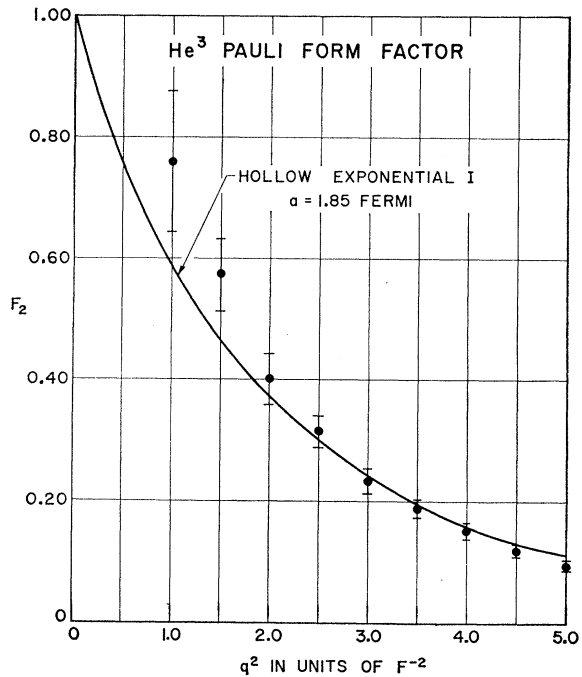


FIG. 15. Hollow exponential I fit to F_2 .

appropriate radii are reduced by approximately 8 and 12%, respectively.

These results make a comparison between He³ and H³ most attractive for further investigation.

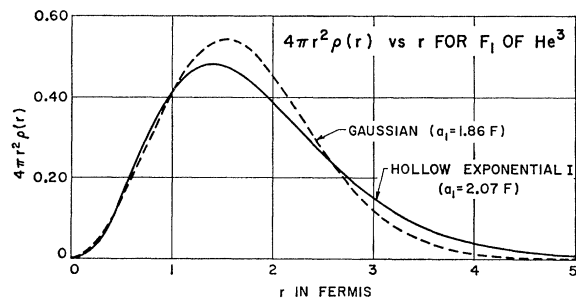


FIG. 16. $4\pi r^2 \rho$ (for F_1) plotted against r for hollow exponential I model and for Gaussian. Total charge equals unity.

A theoretical calculation of the charge radius of He³ was made recently by Pappademos¹⁴ which is in reasonable agreement with the experimental rms values found in our studies. Some theoretical work on the electrodisintegration of He³ has been carried out by Haybron¹⁵ and this will be compared subsequently with the experimental inelastic continua now being studied at Stanford.

¹⁴ J. M. Pappademos, Nucl. Phys. (to be published).

¹⁵ R. M. Haybron (private communication).

ACKNOWLEDGMENTS

We wish to thank Dr. C. deVries for his help in programming solutions of the Rosenbluth equation. We are also grateful to D. Aitken, S. Berezin, P. Bounin, C. Buchanan, C. Crannell, H. Crannell, M. Croissiaux, E. Erickson, P. Gram, E. B. Hughes, T. Janssens, F. Lewis, and M. Yearian for their help in taking some of the experimental data. Dr. Perry Wilson and the operating crew of the linear accelerator have been most helpful to us and we wish to thank them most cordially.

Variational Principles for Electromagnetic Potential Scattering*

R. J. WAGNER

Space Technology Laboratories, Incorporated, Redondo Beach, California

(Received 28 February 1963)

Variational methods are considered for the solution of the vector wave equation describing the field due to an arbitrary source placed in the neighborhood of an inhomogeneous absorbing medium. Variational principles for the tensor Green's function satisfying the point source equation, $\nabla \times \nabla \times \mathbf{\Gamma}(\mathbf{r}, \mathbf{r}') - k^2 \mathbf{\Gamma}(\mathbf{r}, \mathbf{r}') + U(\mathbf{r}) \mathbf{\Gamma}(\mathbf{r}, \mathbf{r}') = -\mathbf{1}\delta(\mathbf{r} - \mathbf{r}')$, have been obtained in linear and exponential forms, analogous to the Altshuler principles for the scalar wave function. Stationary forms for the wave function and the scattering amplitude in the standard scattering problem (incident plane wave, outgoing solutions) are recovered when the point source recedes to infinity. For the special case of a spherically symmetric scatterer, the analysis leads to variational principles for the two independent l th-order phase shifts. The method is illustrated by a calculation of the fields internal to an axially symmetric potential.

I. INTRODUCTION

NEW methods of obtaining approximate solutions to the vector wave equation, based on variational techniques, are presented. The development of variational principles for electromagnetic scattering is, of course, not new, but most of the earlier methods have applied only to surface scattering¹⁻⁵; i.e., the scatterers have been assumed to be perfect conductors. In spite of the considerable interest in scattering by dielectric obstacles, there exist relatively few variational principles applicable directly to the vector-potential-scattering problem. Those that do apply, notably the station-

ary forms based on the "reaction concept" of Rumsey,^{6,7} may be useful in the calculation of cross sections but provide little information on the fields themselves at an arbitrary space point.

The objective of this paper is to present variational principles for the vector-scattering problem which are formal analogs of principles which have been found to be particularly useful in the scalar-scattering theory. In Sec. II, variational principles based on both the differential and integral equations for a generalized tensor Green's function are discussed, and in Sec. III variational principles for the field and dyadic-scattering amplitude are developed. The special case of a spherically symmetric scatterer is considered in Sec. IV, with the analysis leading to amplitude-independent variational principles for the two independent phase shifts required in the vector-scattering problem. An application of the formalism to the scattering of a plane wave by a complex axially symmetric potential is given in Sec. V.

As a slight notational simplification, the following convention is adopted throughout the paper. Unless otherwise specifically indicated, the product of a dyadic

* The research reported in this paper was sponsored by the Air Force Ballistic Systems Division, Air Force Systems Command, under Contract No. AF 04(694)-1 with Space Technology Laboratories, Inc.

¹ The literature on the theory and applications of the variational method to problems of electromagnetic surface scattering is quite extensive, and no attempt will be made to provide an exhaustive list of references. Numerous additional references may be found in those cited in this article.

² H. Levine and J. Schwinger, *Comm. Pure Appl. Math.* **3**, 355 (1950).

³ R. Kiebertz, A. Ishimaru, and G. Held, University of Washington, Department of Electrical Engineering, Tech. Rept. No. 45, 1960 (unpublished).

⁴ R. F. Harrington, *Time-Harmonic Electromagnetic Fields* (McGraw-Hill Book Company, Inc., New York, 1961), Chap. 7.

⁵ J. R. Mentzer, *Scattering and Diffraction of Radio Waves* (Pergamon Press, Inc., New York, 1955).

⁶ V. H. Rumsey, *Phys. Rev.* **94**, 1483 (1954).

⁷ M. H. Cohen, *IRE Trans. Antennas Propagation* **AP-9**, 193 (1955).